Effect of slip on vortex shedding from a circular cylinder in a gas flow

M. A. Gallis* and J. R. Torczynski
Engineering Sciences Center, Sandia National Laboratories, P. O. Box 5800, Albuquerque, New Mexico 87185-0840, USA

(Received 17 February 2021; accepted 1 June 2021; published 21 June 2021)

Most studies of vortex shedding from a circular cylinder in a gas flow have explicitly or implicitly assumed that the no-slip condition applies on the cylinder surface. To investigate the effect of slip, vortex shedding is simulated using molecular gas dynamics (the direct simulation Monte Carlo method) and computational fluid dynamics (the incompressible Navier-Stokes equations with a slip boundary condition). A Reynolds number of 100, a Mach number of 0.3, and a corresponding Knudsen number of 0.0048 are examined. For these conditions, compressibility effects are small, and periodic laminar vortex shedding is obtained. Slip on the cylinder is varied using combinations of diffuse and specular molecular reflections with accommodation coefficients from zero (maximum slip) to unity (minimum slip). Although unrealistic, bounce-back molecular reflections are also examined because they approximate the no-slip boundary condition (zero slip). The results from both methods are in reasonable agreement. The shedding frequency increases slightly as the accommodation coefficient is decreased, and shedding ceases at low accommodation coefficients (large slip). The streamwise and transverse forces decrease as the accommodation coefficient is decreased. Based on the good agreement between the two methods, computational fluid dynamics is used to determine the critical accommodation coefficient below which vortex shedding ceases for Reynolds numbers of 60–100 at a Mach number of 0.3. Conditions to observe the effect of slip on vortex shedding appear to be experimentally realizable, although challenging.

DOI: 10.1103/PhysRevFluids.6.063402

I. INTRODUCTION

Vortex shedding from a circular cylinder in steady flow is one of the iconic problems of fluid mechanics [1]. Since its discovery more than a century ago, this flow has been the subject of many experimental, theoretical, and computational studies, the key results of which are discussed extensively in several review articles [2–4]. For the situation of incompressible flow in an unbounded domain, periodic laminar vortex shedding occurs for Reynolds numbers of 40–150 [4], and accurate expressions for the Strouhal number (nondimensional shedding frequency) are available for Reynolds numbers in this range [5].

Most of these studies have explicitly or implicitly assumed that the no-slip condition applies on the cylinder surface. However, the no-slip condition may not be a good approximation for gas flows under certain conditions. The Knudsen number for an object in a gas flow is not a free parameter but instead is proportional to the Mach number over the Reynolds number, where the proportionality coefficient is approximately 1.6 [6]. Thus, a gas-flow Mach number of 0.3, which is small enough to be almost incompressible, and a cylinder Reynolds number of 100, which is in the range for periodic

*magalli@sandia.gov

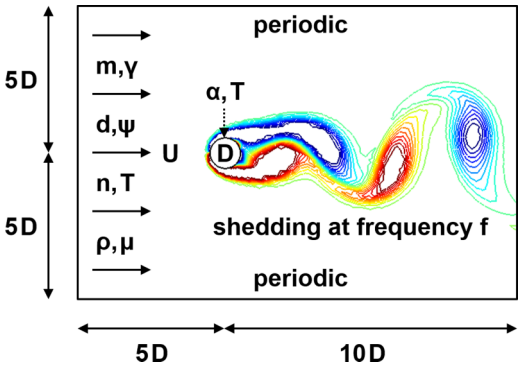

FIG. 1. Conditions for simulating vortex shedding produced by a gas flow over a circular cylinder with slip.

laminar vortex shedding, combine to yield a Knudsen number of 0.0048, which is large enough for non-negligible slip to occur on the cylinder surface.

Relatively few researchers have investigated periodic laminar vortex shedding from an object when slip on the object surface is significant. Bird [6], Usami and Mizuguchi [7], and Tseng *et al.* [8] all simulate vortex shedding from a thin flat plate perpendicular to the gas flow. Due to computational limitations, their domains extend only a few plate widths in the streamwise and transverse directions, their Mach numbers are too large for the flows to be nearly incompressible, and their Reynolds numbers are above the range of interest. Nevertheless, in all of these studies, periodic laminar vortex shedding is observed, but its behavior is not studied in detail.

Usami *et al.* [9] subsequently simulate vortex shedding from a vibrated circular cylinder. Their Mach numbers are low enough to be almost incompressible, and their Reynolds numbers are just slightly above the range of interest. However, their domains are only a few cylinder diameters in the streamwise and transverse directions, and their vibration amplitude in the transverse direction is equal to the cylinder diameter, so the imposed cylinder vibration dominates their situation. They observe lock-in (their phrase) of the vortex shedding at the vibration frequency.

The current investigation extends the preliminary results of Torczynski and Gallis [10], who present simulations of vortex shedding from a circular cylinder with non-negligible slip. Herein, the direct simulation Monte Carlo (DSMC) method of molecular gas dynamics [11–13] and a computational-fluid-dynamics (CFD) implementation of the incompressible Navier-Stokes equations with a slip boundary condition [14–16] are used to simulate vortex shedding from a circular cylinder. Simulations using these two methods are performed at identical flow conditions, allowing direct comparison of their results for vortex shedding with non-negligible slip.

Conditions that yield laminar incompressible flow and produce two-dimensional periodic vortex shedding for no-slip boundaries are examined [4]. The cylinder Reynolds number is 100 or less, which is in this flow regime. The gas flow has a Mach number of 0.3 or less, which produces almost incompressible flow. Slip on the cylinder surface is varied from zero (no-slip) to maximum (zero tangential shear stress) by varying how molecules reflect from the surface [11]. The computational domain used here is two-dimensional and fairly large (although not effectively infinite [4,5]) compared to the cylinder diameter in the streamwise and transverse directions to reduce the effects of inflow, outflow, and blockage. Transient simulations are run for long enough times to observe many vortex-shedding cycles so that the effect of slip on the shedding frequency and the streamwise and transverse forces on the cylinder can be quantified.

II. VORTEX SHEDDING

Figure 1 shows the flow geometry under consideration. The gas has molecular weight m, specific heat ratio γ, molecular collision diameter d, and viscosity temperature exponent ψ [11]. The

gas enters the domain uniformly at the left boundary with number density n, temperature T, and streamwise velocity U. The gas ultimately exits the domain at the right boundary. The upper and lower boundaries are periodic. The cylinder has diameter D. Its center is positioned $5D$ from the inflow boundary (left), $10D$ from the outflow boundary (right), and $5D$ from both of the periodic boundaries (upper and lower). The cylinder surface has accommodation coefficient α that governs molecular reflections [11–13] (discussed in more detail subsequently) and is held at temperature T (i.e., the cylinder temperature equals the freestream gas temperature).

The gas is taken to be ideal with constant specific heat ratio and thus has density ρ, pressure p, and sound speed a, as given below, where k_B is the Boltzmann constant:

$$\rho = mn, \quad p = nk_BT, \quad a = \sqrt{\gamma k_BT/m}. \tag{1}$$

Herein, the molecular mean free path λ is defined in terms of the viscosity μ, the density ρ, and the molecular speed scale c [15,16]:

$$\lambda = \frac{2\mu}{\rho c}, \quad c = \sqrt{\frac{8k_BT}{\pi m}}. \tag{2}$$

This generic expression differs by only 0.25% from the exact infinite-approximation Chapman-Enskog value for hard-sphere molecular collisions (which are considered subsequently) [17,18]. Hard-sphere, variable-hard-sphere, and variable-soft-sphere molecular collisions [11] all lead to the following temperature dependence for the viscosity μ and the thermal conductivity K, where the Prandtl number Pr and the specific heat C_p are constant and "ref" denotes a reference state:

$$\frac{\mu}{\mu_{\text{ref}}} = \frac{K}{K_{\text{ref}}} = \left(\frac{T}{T_{\text{ref}}}\right)^{\psi}, \quad \text{Pr} = \frac{\mu C_P}{K}, \quad C_p = \frac{\gamma}{\gamma - 1}\frac{k_B}{m}. \tag{3}$$

The Reynolds, Mach, and Knudsen numbers for this situation are given below and are interdependent based on the above expressions:

$$\text{Re} = \frac{\rho U D}{\mu}, \quad \text{Ma} = \frac{U}{a}, \quad \text{Kn} = \frac{\lambda}{D} = \sqrt{\frac{\pi\gamma}{2}}\frac{\text{Ma}}{\text{Re}}. \tag{4}$$

The nondimensional time $\hat{t}$, frequency $\hat{f}$ (the Strouhal number Sr), and force per unit length $\hat{\mathbf{F}}$ on the cylinder are given below:

$$\hat{t} = \frac{Ut}{D}, \quad \hat{f} = \frac{fD}{U} = \text{Sr}, \quad \hat{\mathbf{F}} = \frac{\mathbf{F}/L}{\rho U^2 D}. \tag{5}$$

III. NUMERICAL METHODS

A. Direct simulation Monte Carlo (DSMC)

Bird's direct simulation Monte Carlo (DSMC) method [11–13] of molecular gas dynamics is used to simulate vortex shedding from a circular cylinder. DSMC uses "particles" (computational molecules) to represent a gas flow. Each particle represents a large number of actual gas molecules. These particles move ballistically, reflect from solid boundaries, and collide stochastically in a pairwise fashion so as to reproduce the statistical behavior of actual molecules. Sampling the properties of the particles within each cell yields the flow properties for that cell. Typically, the cell size and the time step are much smaller than the molecular mean free path and the molecular mean collision time, respectively. Like most molecular methods, DSMC is "noisy": flow quantities associated with a cell fluctuate as particles move into and out of the cell. However, since the time step is typically orders of magnitude smaller than the flow time scales of interest, statistical noise is reduced to low levels by averaging cell-based quantities over many time steps while still resolving transient flows [11].

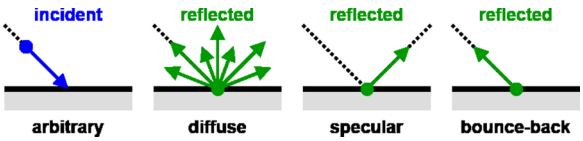

FIG. 2. Processes employed for molecular reflection from the cylinder surface.

Sandia's open-source massively parallel DSMC code SPARTA [12,13] is used to perform these simulations. SPARTA has been extensively validated for flows in the near-continuum regime [12,13] and has been recently applied to instabilities and turbulent flows in this regime [19–22]. The gas is like argon in that it has molecular mass $m = 66.3 \times 10^{-27}$ kg, specific heat ratio $\gamma = 5/3$ (a monatomic gas), and viscosity $\mu = 2.117 \times 10^{-5}$ Pa s at temperature $T = 273.15$ K [11]. However, hard-sphere molecular collisions are performed, so the viscosity temperature exponent is $\psi = 1/2$ instead of an empirical value for argon such as 0.81 [11]. At these conditions, the sound speed and the molecular speed scale are $a = 307.9\,\mathrm{m/s}$ and $c = 380.6\,\mathrm{m/s}$, respectively. The cylinder diameter is chosen to be $D = 1$ m for convenience.

The Mach and Reynolds numbers are prescribed to be $\mathrm{Ma} = 0.3$ and $\mathrm{Re} = 100$, which yield a Knudsen number of $\mathrm{Kn} = 0.0048$. Thus, the freestream velocity, density, number density, and molecular mean free path are $U = 92.37\,\mathrm{m/s}$, $\rho = 2.292 \times 10^{-5}\,\mathrm{kg/m^3}$, $n = 3.457 \times 10^{20}\,1/\mathrm{m^3}$, and $\lambda = 0.0048\,\mathrm{m}$, respectively. The computational domain is two-dimensional and extends 15 m in the streamwise direction and 10 m in the transverse direction. This domain is meshed using about 80 million square cells of side length $\Delta s = 0.00137\,\mathrm{m}$, which is about 1/4 of the mean free path. The time step is $\Delta t = 1.48 \times 10^{-6}$ s, which is less than 1/4 of the mean collision time. These cells are initially filled with an average of 100 particles per cell, for a total of about 8 billion particles. The cylinder surface (a circle) is represented by 10 333 equally spaced straight-line segments.

Figure 2 shows the processes employed for molecular reflection from the cylinder surface. The main process employed is a linear combination of diffuse reflection at the cylinder temperature with probability α plus specular reflection with probability $1 - \alpha$ [11]. Nine values of the accommodation coefficient α between 0 and 1 are simulated, where $\alpha = 0$ is the specular limit (maximum slip) and $\alpha = 1$ is the diffuse fully accommodating limit (minimum slip). Although physically unrealistic, bounce-back molecular reflections (zero slip) are also examined because they approximate the no-slip boundary condition and thus can be used to gauge the effect of slip on vortex shedding. Here, when applied to slip, the terms maximum, minimum, and zero describe the sums of the tangential velocity components of the incident and reflected molecules.

Most of these DSMC simulations are performed on Sequoia, an IBM Blue Gene/Q supercomputer formerly at Lawrence Livermore National Laboratory, and typically use 32k nodes with 16 cores per node and four threads per core (i.e., about 2 million threads total) for 30 h.

B. Computational fluid dynamics (CFD)

Computational fluid dynamics (CFD) is also used to simulate vortex shedding from a circular cylinder. More specifically, the transient incompressible Navier-Stokes equations are used with a slip boundary condition on the cylinder. The gas properties, computational domain, and boundary conditions are the same or equivalent to those used in the DSMC simulations (Fig. 1). Since the Mach number is low and the boundaries are isothermal, compressibility effects are small and thus neglected.

A slip boundary condition is used on the cylinder. The normal velocity component u_n is zero, and the tangential shear stress τ_t is proportional to the tangential velocity component u_t. The coefficient of proportionality is found by comparing CFD and DSMC simulations of Couette and Poiseuille flows [15,16] for accommodation values covering the range $0 \leqslant \alpha \leqslant 1$. This approach yields a slip

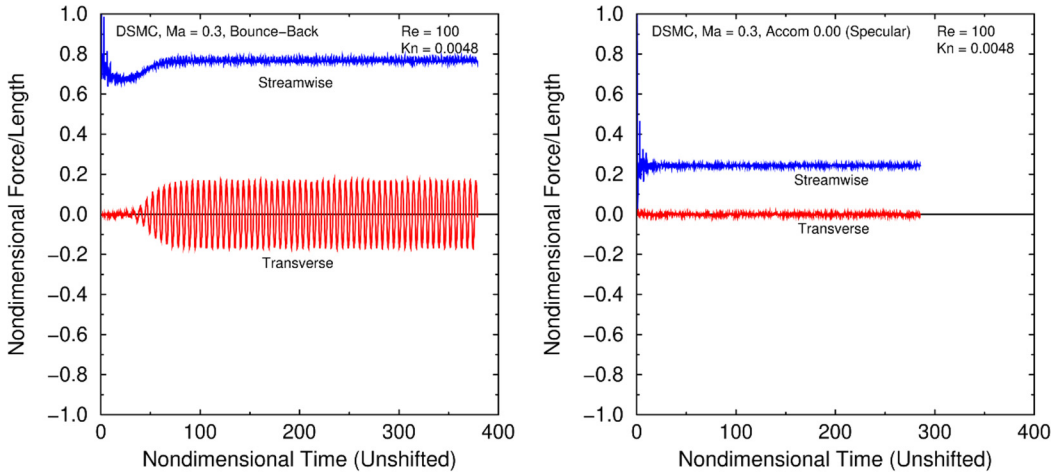

FIG. 3. DSMC force histories for bounce-back (left) and specular (right) molecular reflections. By a nondimensional time of ∼100, either periodic vortex shedding or steady flow is established.

boundary condition, where $d_1 = 0.136$ for hard-sphere collisions ($\psi = 1/2$) [15,16]:

$$\tau_t = \frac{\alpha \rho c u_t}{2(2-\alpha)(1+d_1\alpha)}, \quad u_n = 0. \tag{6}$$

COMSOL Multiphysics [14] is used to perform these CFD simulations. Small time steps and a highly refined mesh with quadratic velocity shape functions are used to obtain accurate results for the vortex-shedding frequency and the cylinder forces. The accommodation coefficient α is varied from 0 (maximum slip) to 1 (minimum slip) in increments of 0.05. The no-slip boundary condition (zero slip) is also simulated to gauge the effect of slip on vortex shedding.

IV. SIMULATION RESULTS

Figure 3 shows DSMC simulation results for the streamwise and transverse components of the nondimensional force per unit length for bounce-back and specular molecular reflections. The DSMC simulations are initialized by applying the inflow conditions to every cell in the domain. As a result, the initial transverse force is basically zero, and the initial streamwise force is large. This initial flow field rapidly adjusts to the presence of the cylinder. For bounce-back reflections, flow oscillations begin almost immediately, and periodic vortex shedding is established by a nondimensional time of ∼100. Once this situation is achieved, the streamwise and transverse forces have nonzero oscillating components, and the streamwise force has a nonzero mean component. The DSMC force histories for accommodation-coefficient values in the range $0.10 \leqslant \alpha \leqslant 1.00$ also exhibit these features. However, for $\alpha = 0.00$ (specular reflections) and $\alpha = 0.05$, no oscillations appear. Instead, steady flow is established well before a nondimensional time of ∼100.

Figure 4 shows the DSMC and CFD force histories after either periodic vortex shedding or steady flow is established. In these plots, the results are shifted to align their phases at zero time. Although not identical, the DSMC and CFD results agree surprisingly well, despite the fact that the assumption of small compressibility is somewhat marginal for a Mach number of Ma = 0.3. For both methods, as slip is increased (i.e., as accommodation is decreased), the vortex-shedding frequency increases, but the streamwise and transverse forces both decrease. The simulations with zero slip (DSMC with bounce-back reflections and CFD with the no-slip boundary condition) follow these same trends and yield the lowest vortex-shedding frequencies and the highest streamwise and transverse forces. The quantitative values for the vortex-shedding frequency and the streamwise

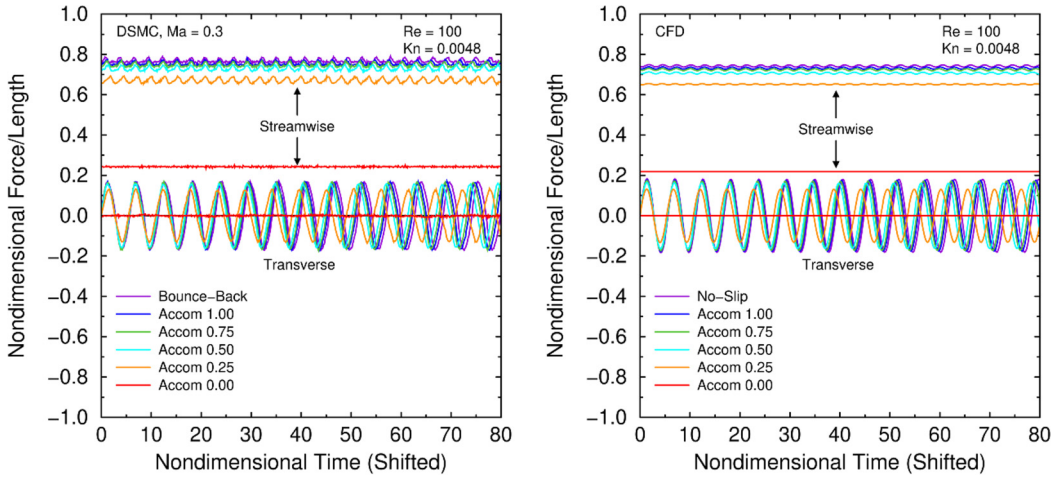

FIG. 4. DSMC (left) and CFD (right) force histories at late times with periodic vortex shedding. The frequency and the amplitude for both methods depend similarly on the amount of slip.

and transverse forces that are discussed below and shown in subsequent figures are extracted from Fourier analysis of the data sets shown in these two graphs.

Figure 5 quantifies how the vortex-shedding frequency depends on slip for both methods. As minimum slip (unity accommodation) is approached, the DSMC and CFD frequencies decrease toward their corresponding zero-slip frequencies (bounce-back for DSMC and no-slip for CFD). As the opposite limit of maximum slip (zero accommodation) is approached, the DSMC and CFD frequencies increase slightly above their corresponding zero-slip frequencies by similar amounts. Vortex shedding ceases completely for large slip (small accommodation). Based on both the DSMC and CFD results, the critical accommodation coefficient corresponding to this transition lies in the range $0.05 \leqslant \alpha \leqslant 0.10$. The zero-slip frequencies lie slightly above the value $\mathrm{Sr} = 0.165$ obtained for $\mathrm{Re} = 100$ from the correlation of Fey *et al.* [5]. The reason for this difference is that their correlation applies for domains of large streamwise and transverse extents, whereas the present

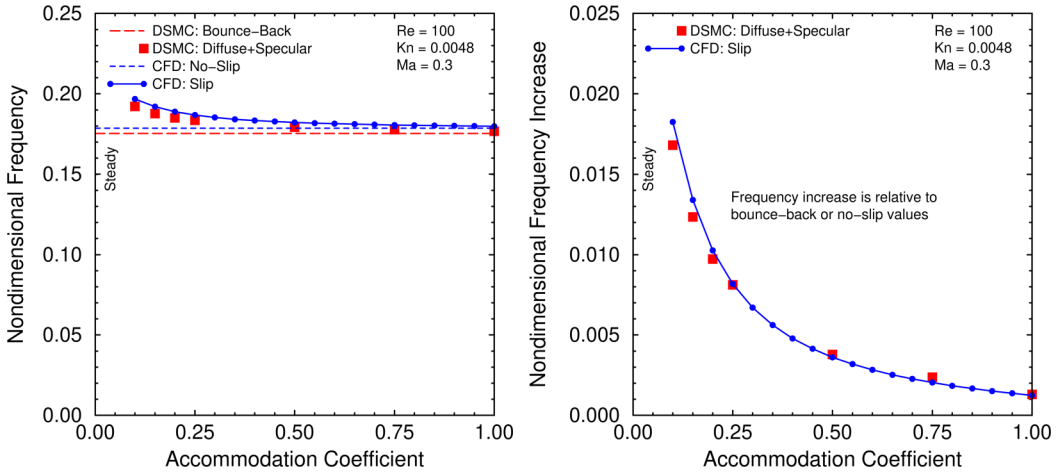

FIG. 5. DSMC and CFD vortex-shedding frequencies versus accommodation. Both methods yield frequencies that increase similarly with increasing slip (decreasing accommodation).

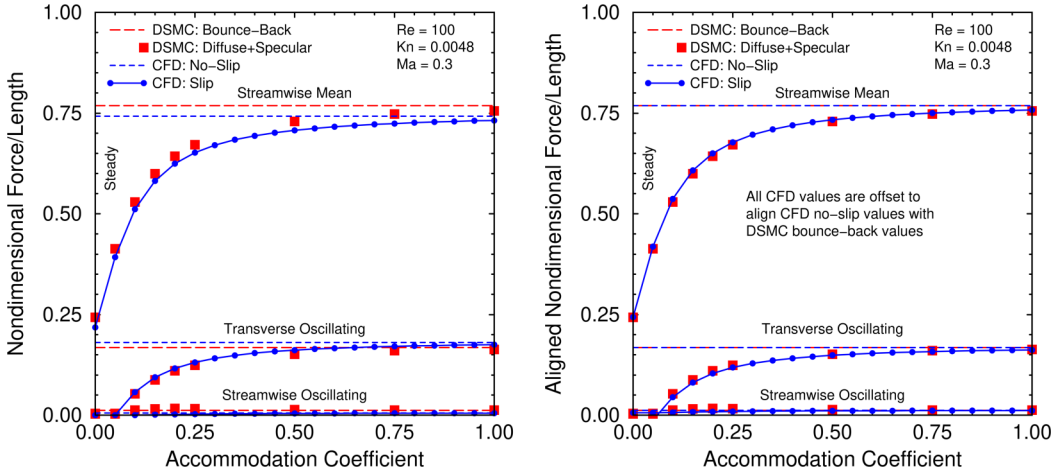

FIG. 6. DSMC and CFD forces versus accommodation. Both methods yield forces that decrease similarly with increasing slip (decreasing accommodation) relative to zero-slip values.

simulations use a domain of only modest streamwise and transverse extents. Additional CFD simulations using the no-slip boundary condition and domains of progressively larger extents do yield frequencies that closely approach the correlation value.

Figure 6 quantifies how various forces on the cylinder depend on slip for both methods. Three force quantities are plotted in each graph: the mean (time-average) of the streamwise force, the amplitude of the oscillating transverse force, and the amplitude of the oscillating streamwise force (the mean transverse force is zero). As minimum slip (unity accommodation) is approached, all three DSMC and CFD force quantities increase toward their corresponding zero-slip values (bounce-back for DSMC and no-slip for CFD). As the opposite limit of maximum slip (zero accommodation) is approached, all three DSMC and CFD force quantities decrease significantly below their corresponding zero-slip values. As stated earlier, vortex shedding ceases completely for large slip (small accommodation). This transition is observed most easily in the oscillating transverse force amplitude, which is zero below this point. Again, based on both the DSMC and CFD results, the critical accommodation coefficient corresponding to this transition lies in the range $0.05 \leqslant \alpha \leqslant 0.10$. The mean streamwise force at maximum slip (zero accommodation) is roughly one quarter of its value at minimum slip (unity accommodation) for these conditions.

To demonstrate that the DSMC and CFD results agree more closely as the continuum limit is approached, each method is applied to perform an additional simulation with minimum slip (unity accommodation) for $\mathrm{Re} = 100$ but at $\mathrm{Ma} = 0.1$ and hence $\mathrm{Kn} = 0.0016$ instead of $\mathrm{Ma} = 0.3$ and hence $\mathrm{Kn} = 0.0048$. Unlike the CFD method, the DSMC method requires significantly more computational resources to simulate $\mathrm{Ma} = 0.1$ than it does to simulate $\mathrm{Ma} = 0.3$. For $\mathrm{Ma} = 0.1$, $\mathrm{Re} = 100$, and $\mathrm{Kn} = 0.0016$, the domain is meshed using about 720 million square cells of side length $\Delta s = 0.000456\,\mathrm{m}$, which is about $1/4$ of the mean free path. These cells are initially filled with an average of 100 particles per cell, for a total of about 72 billion particles, about nine times the number in the $\mathrm{Ma} = 0.3$ simulation. A time step of $\Delta t = 1.48 \times 10^{-6}$ s is used, which is about $1/3$ of the mean collision time. The $\mathrm{Ma} = 0.1$ DSMC simulation is also performed on Sequoia using 32k nodes with 16 cores per node and four threads per core (about 2 million threads total), but 300 h is required, whereas only 30 h is required for each $\mathrm{Ma} = 0.3$ DSMC simulation.

Figure 7 compares force histories at $\mathrm{Ma} = 0.3$ and $\mathrm{Ma} = 0.1$ obtained from both methods. The DSMC and CFD vortex-shedding frequencies and force quantities are closer for $\mathrm{Ma} = 0.1$ than for $\mathrm{Ma} = 0.3$. These trends are as expected because compressibility and slip effects are smaller for $\mathrm{Ma} = 0.1$ and $\mathrm{Kn} = 0.0016$ than for $\mathrm{Ma} = 0.3$ and $\mathrm{Kn} = 0.0048$. The DSMC force histories

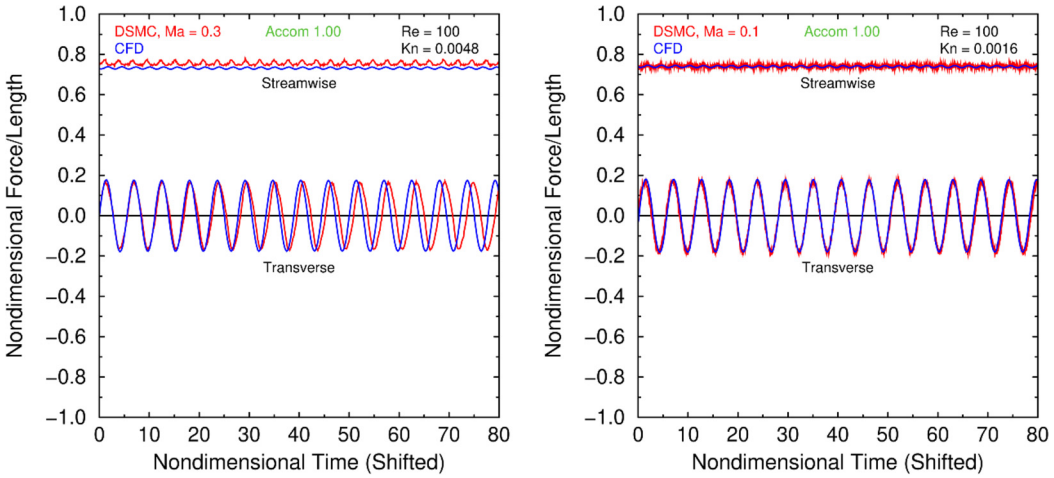

FIG. 7. DSMC and CFD forces at Ma = 0.3 (left) and Ma = 0.1 (right) for an accommodation of unity. The frequencies and amplitudes agree more closely at lower Mach and Knudsen numbers.

are noisier for Ma = 0.1 than for Ma = 0.3 because the ratios of flow to molecular quantities are smaller [11]. Figure 8 shows the DSMC and CFD velocity fields for Ma = 0.1 at the same time in the oscillation cycle. The velocity fields are almost identical except near the outflow boundary, on which DSMC applies the inlet flow conditions [11] but CFD applies zero pressure and zero viscous stress [14]. As a result, in the DSMC simulations, vortices are attenuated more as they exit the

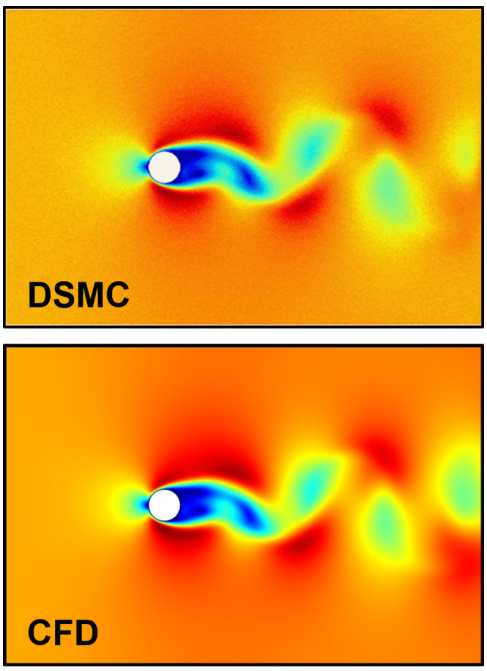

FIG. 8. DSMC (upper) and CFD (lower) velocity fields at Ma = 0.1 and unity accommodation.

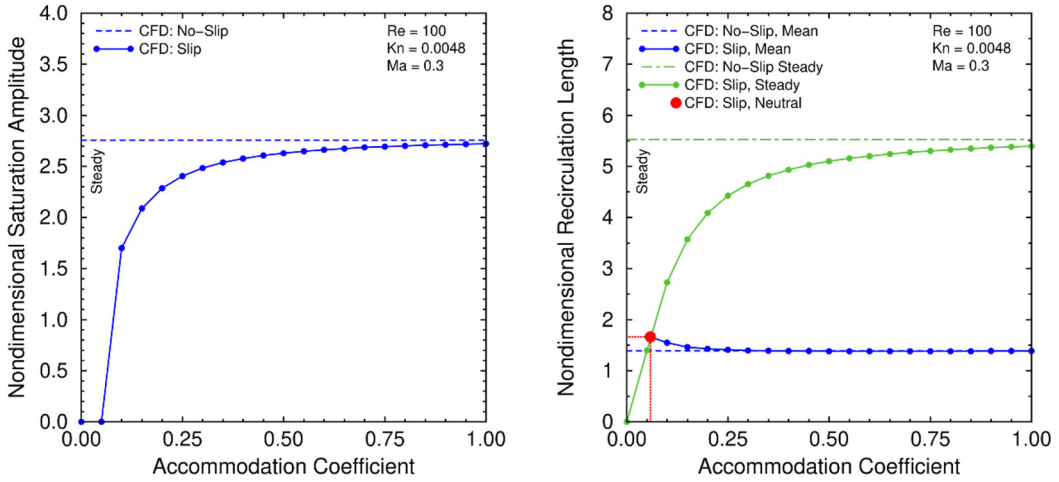

FIG. 9. CFD results for the saturation amplitude and the mean and steady recirculation lengths (points of zero velocity on the centerline) versus accommodation coefficient.

domain. Nevertheless, the good agreement upstream of this boundary indicates that it is far enough downstream from the cylinder to avoid affecting the shedding process significantly.

V. INSTABILITY CHARACTERIZATION

Given the good agreement between the CFD and DSMC results, CFD can be used with confidence to characterize the effect of slip on the vortex-shedding instability in greater detail than is possible using DSMC, which requires substantial computational resources for such simulations. Many aspects of the supercritical Hopf bifurcation associated with the onset of vortex shedding have been characterized in great detail over the last several decades [23–27]. To quantify the effect of slip on the vortex-shedding instability at this level of detail is beyond the scope of this study. Nevertheless, in the hope of encouraging further computational, theoretical, and/or experimental investigations of this regime, CFD is applied below to generate a few selected results of interest.

One quantity of interest for the vortex-shedding instability is the saturation amplitude, namely the strength of the oscillating portion of the flow field after it has become fully established. The saturation amplitude is determined from direct numerical simulation (DNS) and/or theory [26,27] in the following manner. Velocity, position, and time are nondimensionalized as follows:

$$\hat{\mathbf{u}} = \frac{\mathbf{u}}{U}, \quad \hat{\mathbf{x}} = \frac{\mathbf{x}}{D}, \quad \hat{t} = \frac{Ut}{D}. \tag{7}$$

The velocity field is decomposed into steady and oscillating portions, where $\langle \cdots \rangle$ denotes the time average over one cycle:

$$\hat{\mathbf{u}}[\hat{\mathbf{x}}, \hat{t}] = \bar{\mathbf{u}}[\hat{\mathbf{x}}] + \tilde{\mathbf{u}}[\hat{\mathbf{x}}, \hat{t}], \quad \langle \tilde{\mathbf{u}} \rangle = \mathbf{0}. \tag{8}$$

In harmony with previous work [27], the saturation amplitude is defined as follows, where the integral is over the two-dimensional computational domain shown in Fig. 1:

$$A = \left\{ 2 \int \langle \tilde{\mathbf{u}} \cdot \tilde{\mathbf{u}} \rangle d\hat{x} d\hat{y} \right\}^{1/2}. \tag{9}$$

Figure 9 shows the saturation amplitude A for $\mathrm{Re} = 100$ and $\mathrm{Ma} = 0.3$ as a function of the accommodation coefficient α. The no-slip value in this figure is in reasonable agreement with the corresponding DNS value found by other investigators using a somewhat larger domain [27].

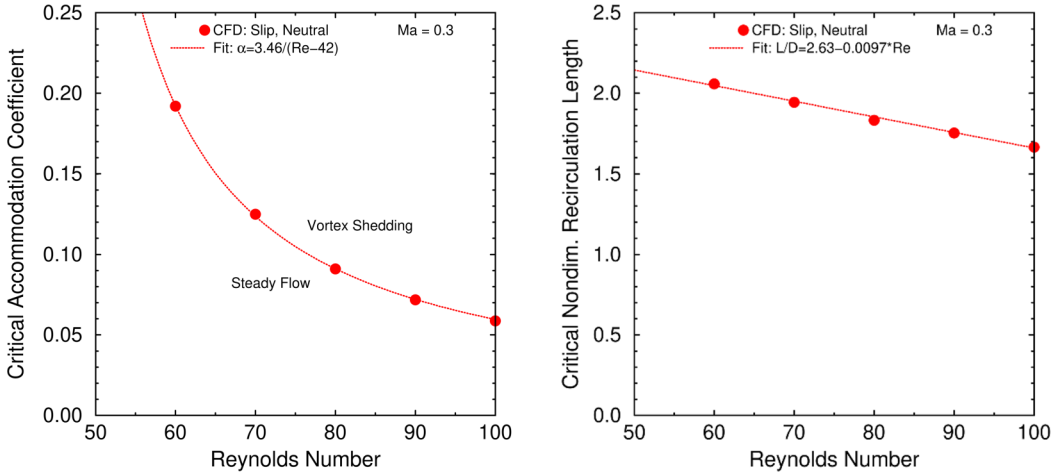

FIG. 10. CFD results for the critical accommodation coefficient (below which vortex shedding ceases) and the recirculation length at this value (the neutral condition) as functions of the Reynolds number, with curves drawn to guide the eye.

Unsurprisingly, as slip increases (accommodation decreases), the saturation amplitude decreases and vanishes within $0.05 \leqslant \alpha \leqslant 0.10$, as expected from the CFD results for the oscillating force. Although, in principle, the critical accommodation coefficient could be determined by performing more simulations in this range, in practice it becomes difficult to determine whether the instability is growing or decaying because the growth or decay rate becomes extremely small.

Figure 9 illustrates a better method for determining the critical accommodation coefficient. This method involves comparing the recirculation lengths of the mean velocity field and the corresponding steady velocity field [26]. The neutral condition is realized when these two recirculation lengths are equal, and this intersection point, which is easily found, yields the critical accommodation coefficient. For $\mathrm{Re} = 100$ and $\mathrm{Ma} = 0.3$, this critical value is $\alpha = 0.059$.

Figure 10 shows the results of carrying out the process illustrated in Fig. 9 for additional values of the Reynolds number. In all cases, the Mach number is maintained at $\mathrm{Ma} = 0.3$. Thus, as the Reynolds number is decreased below 100, the Knudsen number is increased above 0.0048, so the effect of slip is expected to increase correspondingly. Unsurprisingly, as slip increases (here, as the Reynolds number decreases), the critical accommodation coefficient increases as well. In other words, as the Knudsen number is increased, the flow becomes progressively more stable. Curiously, the variation of the critical accommodation coefficient with Reynolds number is found to be well represented by an inverse dependence, as indicated in the legend of the left plot. Moreover, the asymptote of 42 is close to the no-slip critical Reynolds number value of $\sim$47. At present, no theoretical justifications for these behaviors are known. The recirculation length at the neutral condition is seen to increase weakly with increasing slip (decreasing Reynolds number). These trends could serve as useful guides for more detailed investigations in the future.

VI. EXPERIMENTAL REALIZABILITY

A reasonable question at this point is why the effect of slip on vortex shedding has not been previously reported. The answer is that slip is important only in rather narrow parameter ranges. The Reynolds number must be around 100 because the flow is steady at lower values [4] and slip is small at higher values. Similarly, the Mach number must be around 0.3 because slip is small at lower values and compressible effects dominate at higher values. Thus, $\mathrm{Re} = 100$, $\mathrm{Ma} = 0.3$, and hence $\mathrm{Kn} = 0.0048$ (for a monatomic gas with $\gamma = 5/3$) are reasonable baseline values. Under

these conditions, when shedding occurs, the Strouhal number is approximately $\mathrm{Sr} \approx 0.2$ so long as the accommodation coefficient satisfies $0.2 \leqslant \alpha \leqslant 1.0$, based on the present study.

The simulations here use a cylinder diameter of $D = 1\,\mathrm{m}$ and thus a domain of $15\,\mathrm{m} \times 10\,\mathrm{m}$ simply for convenience, but such a large geometry is not practical for performing experiments. A diameter of $D = 0.01\,\mathrm{m}$ is a reasonable baseline because experimenters have used cylinders of similar diameters (e.g., fabricated from precision drill rods) [28]. Although other materials might be feasible, metal cylinders are promising due to their strength, stiffness, and smoothness [28] (surface roughness should be small compared to the below values of the molecular mean free path). Moreover, common metals such as stainless steel and aluminum have large thermal conductivities, which facilitates ensuring that the surface is isothermal. Temperature control could be enhanced by using a hollow cylinder through which liquid at a prescribed temperature is circulated. Again, practical considerations suggest that the gas and cylinder temperature not differ significantly from ambient conditions, so $T = 273.15\,\mathrm{K}$ is a reasonable baseline temperature.

The accommodation coefficient is controlled primarily through the choice of gas and the choice of cylinder material. Trott *et al.* [29,30] have shown that argon, nitrogen, and helium have accommodation coefficients of ∼0.9, ∼0.8, and ∼0.4, respectively, with aluminum, stainless steel, and gold-coated stainless steel. Thus, argon and helium are good baseline choices for the gas.

Argon has molecular mass $m = 66.3 \times 10^{-27}\,\mathrm{kg}$, viscosity temperature exponent $\psi = 0.81$, and viscosity $\mu = 2.117 \times 10^{-5}\,\mathrm{Pa\,s}$ at temperature $T = 273.15\,\mathrm{K}$ [11]. For $\mathrm{Re} = 100$, $\mathrm{Ma} = 0.3$, and $\mathrm{Kn} = 0.0048$, the following freestream values are obtained: sound speed $a = 307.9\,\mathrm{m/s}$, velocity $U = 92.37\,\mathrm{m/s}$, density $\rho = 2.292 \times 10^{-3}\,\mathrm{kg/m^3}$, pressure $p = 130\,\mathrm{Pa}$, and molecular mean free path $\lambda = 0.000048\,\mathrm{m}$. The slip boundary condition should use the value $d_1 = 0.165$ instead of the hard-sphere value [15,16], but this has little effect. For a Strouhal number $\mathrm{Sr} \approx 0.2$, the vortex-shedding frequency is $f \approx 2\,\mathrm{kHz}$, which is not unreasonably high.

Helium has molecular mass $m = 6.65 \times 10^{-27}\,\mathrm{kg}$, viscosity temperature exponent $\psi = 0.66$, and viscosity $\mu = 1.865 \times 10^{-5}\,\mathrm{Pa\,s}$ at temperature $T = 273.15\,\mathrm{K}$ [11]. For $\mathrm{Re} = 100$, $\mathrm{Ma} = 0.3$, and $\mathrm{Kn} = 0.0048$, the following freestream values are obtained: sound speed $a = 972.2\,\mathrm{m/s}$, velocity $U = 291.66\,\mathrm{m/s}$, density $\rho = 6.394 \times 10^{-4}\,\mathrm{kg/m^3}$, pressure $p = 363\,\mathrm{Pa}$, and molecular mean free path $\lambda = 0.000048\,\mathrm{m}$. The slip boundary condition should use the value $d_1 = 0.165$ instead of the hard-sphere value [15,16], but this has little effect. For a Strouhal number $\mathrm{Sr} \approx 0.2$, the vortex-shedding frequency is $f \approx 6\,\mathrm{kHz}$, which is not unreasonably high.

The effect of slip at fixed Reynolds number can be determined by systematically increasing the density ρ and decreasing the velocity U while keeping the product ρU fixed (as above). Thus, the Reynolds number remains fixed, but the Mach and Knudsen numbers are both correspondingly reduced. Large enough reductions of these two parameters can decrease slip on the cylinder surface to the point that the no-slip condition again becomes a good approximation. While challenging, the above flow conditions should be experimentally realizable. However, they would probably be chosen only if the effect of slip were the particular focus of the investigation.

VII. CONCLUSIONS

Slip at the surface of a cylinder in a gas flow can significantly affect vortex shedding. As the degree of slip is increased, the vortex-shedding frequency increases modestly, and the streamwise and transverse forces on the cylinder decrease significantly. Moreover, when the degree of slip becomes large enough (close to zero tangential shear stress), vortex shedding ceases. As the degree of slip is decreased, the frequency and the forces approach their no-slip values.

These phenomena are demonstrated using numerical simulations of vortex shedding at a Reynolds number of 100 and a Mach number of 0.3, which lead to a Knudsen number of 0.0048. The fact that two different simulation methods (DSMC and CFD) produce the same phenomena is good evidence that these phenomena are real, rather than being numerical artifacts. Furthermore, the good agreement of CFD with DSMC indicates that the slip regime can be explored thoroughly using CFD instead of DSMC, which, since it is a molecular method, is computationally intense.

More specifically, the slip boundary condition used in the CFD simulations gives good agreement with the DSMC simulations over the entire range of slip, from minimum (unity accommodation) to maximum (zero accommodation).

Based on this good agreement, additional CFD simulations at Reynolds numbers of 60–100 and a Mach number of 0.3 are performed to characterize selected aspects of the vortex-shedding instability. Of particular interest is the critical accommodation coefficient, below which vortex shedding ceases. This quantity is found to increase with decreasing Reynolds number, which, at fixed Mach number, corresponds to increasing Knudsen number and thus to increasing slip.

The effect of slip on vortex shedding does not appear to have been reported previously. The reason for this appears to be that slip is significant only in rather narrow parameter ranges. The Reynolds number must be around 100 because the flow is steady at lower values and slip is small at higher values. Similarly, the Mach number must be around 0.3 because slip is small at lower values and compressible effects dominate at higher values. Employing argon or helium with laboratory-size cylinders (e.g., 1 cm diameter) made of common metals (i.e., aluminum or stainless steel) yields experimental conditions that are challenging but probably realizable.

ACKNOWLEDGMENTS

The authors thank T. P. Koehler and R. M. McMullen of Sandia National Laboratories for helpful discussions about this research and its presentation herein.

Sandia National Laboratories is a multimission laboratory managed and operated by National Technology and Engineering Solutions of Sandia, LLC, a wholly owned subsidiary of Honeywell International, Inc., for the U.S. Department of Energy's National Nuclear Security Administration under contract DE-NA0003525.

This paper describes objective technical results and analysis. Any subjective views or opinions that might be expressed in the paper do not necessarily represent the views of the U.S. Department of Energy or the United States Government.

This manuscript has been authored by National Technology and Engineering Solutions of Sandia, LLC, under Contract No. DE-NA0003525 with the U.S. Department of Energy. The United States Government retains and the publisher, by accepting the article for publication, acknowledges that the United States Government retains a nonexclusive, paid-up, irrevocable, world-wide license to publish or reproduce the published form of this manuscript, or allow others to do so, for United States Government purposes.

[1] M. Van Dyke, *An Album of Fluid Motion* (Parabolic Press, Stanford, CA, 1982).

[2] M. Morkovin, Flow around circular cylinders—A kaleidoscope of challenging fluid phenomena, in *Proceedings of the ASME Symposium on Fully Separated Flows*, edited by A. D. Hansen (American Society of Mechanical Engineers, Philadelphia, PA, 1964), pp. 102–118.

[3] E. Berger and R. Wille, Periodic flow phenomena, Annu. Rev. Fluid Mech. **4**, 313 (1972).

[4] C. H. K. Williamson, Vortex dynamics in the cylinder wake, Annu. Rev. Fluid Mech. **28**, 477 (1996).

[5] U. Fey, M. König, and H. Eckelmann, A new Strouhal-Reynolds-number relationship for the circular cylinder in the range $47 < \mathrm{Re} < 2 \times 10^5$, Phys. Fluids **10**, 1547 (1998).

[6] G. A. Bird, Knudsen and Mach number effects on the development of wake instabilities, in *Proceedings of the 36th AIAA Aerospace Sciences Meeting and Exhibit* (AIAA, Reston, VA, 1998), Paper No. AIAA-98-0785.

[7] M. Usami and K. Mizuguchi, DSMC calculation of vortex shedding behind a flat plate with a new intermolecular collision scheme, AIP Conf. Proc. **762**, 686 (2005).

[8] K. C. Tseng, T. C. Kuo, S. C. Lin, C. C. Su, and J. S. Wu, Simulations of subsonic vortex-shedding flow past a 2D vertical plate in the near-continuum regime by the parallelized DSMC code, Comput. Phys. Commun. **183**, 1596 (2012).

[9] M. Usami, T. Kamiya, H. Maeda, and Y. Furukawa, DSMC calculation of Karman vortex flow and Taylor vortex flow by an improved new collision scheme (U-system 3), AIP Conf. Proc. **1084**, 365 (2008).
[10] J. R. Torczynski and M. A. Gallis, DSMC simulation of flow past a circular cylinder at Re = 100, BAPS **64**, B12.00005 (2019).
[11] G. A. Bird, *Molecular Gas Dynamics and the Direct Simulation of Gas Flows* (Clarendon Press, Oxford, UK, 1998).
[12] M. A. Gallis, T. P. Koehler, and S. J. Plimpton, *SPARTA Stochastic Particle Real Time Analyzer Validation and Verification Test Suite*, SAND2014-19198 (Sandia National Laboratories, Albuquerque, NM, 2014).
[13] S. J. Plimpton, S. G. Moore, A. Borner, A. K. Stagg, T. P. Koehler, J. R. Torczynski, and M. A. Gallis, DSMC on petascale machines and beyond, Phys. Fluids **31**, 086101 (2019).
[14] *COMSOL AB, COMSOL Multiphysics User's Guide,Version 3.5a* (COMSOL AB, Stockholm, Sweden, 2008).
[15] J. R. Torczynski and M. A. Gallis, DSMC-based shear-stress/velocity-slip boundary condition for Navier-Stokes Couette-flow simulations, AIP Conf. Proc. **1333**, 802 (2011).
[16] M. A. Gallis and J. R. Torczynski, Direct simulation Monte Carlo-based expressions for the gas mass flow rate and pressure profile in a microscale tube, Phys. Fluids **24**, 012005 (2012).
[17] S. Chapman and T. G. Cowling, *The Mathematical Theory of Non-Uniform Gases* (Cambridge University Press, Cambridge, 1970).
[18] M. A. Gallis, J. R. Torczynski, and D. J. Rader, Molecular gas dynamics observations of Chapman-Enskog behavior and departures therefrom in nonequilibrium gases, Phys. Rev. E **69**, 042201 (2004).
[19] M. A. Gallis, T. P. Koehler, J. R. Torczynski, and S. J. Plimpton, Direct simulation Monte Carlo investigation of the Richtmyer-Meshkov instability, Phys. Fluids **27**, 084105 (2015).
[20] M. A. Gallis, T. P. Koehler, J. R. Torczynski, and S. J. Plimpton, Direct simulation Monte Carlo investigation of the Rayleigh-Taylor instability, Phys. Rev. Fluids **1**, 043403 (2016).
[21] M. A. Gallis, N. P. Bitter, T. P. Koehler, J. R. Torczynski, S. J. Plimpton, and G. Papadakis, Molecular-Level Simulations of Turbulence and Its Decay, Phys. Rev. Lett. **118**, 064501 (2017).
[22] M. A. Gallis, J. R. Torczynski, M. C. Krygier, N. P. Bitter, and S. J. Plimpton, Turbulence at the edge of continuum, Phys. Rev. Fluids **6**, 013401 (2021).
[23] P. Huerre and P. A. Monkewitz, Local and global instabilities in spatially developing flows, Annu. Rev. Fluid Mech. **22**, 473 (1990).
[24] J. Dušek, P. Le Gal, and P. Fraunié, A numerical and theoretical study of the first Hopf bifurcation in a cylinder wake, J. Fluid Mech. **264**, 59 (1994).
[25] B. J. A. Zielinska and J. E. Wesfreid, On the spatial structure of global modes in wake flow, Phys. Fluids **7**, 1418 (1995).
[26] B. J. A. Zielinska, S. Goujon-Durand, J. Dušek, and J. E. Wesfreid, Strongly Nonlinear Effect in Unstable Wakes, Phys. Rev. Lett. **79**, 3893 (1997).
[27] V. Mantič-Lugo, C. Arratia, and F. Gallaire, Self-Consistent Mean Flow Description of the Nonlinear Saturation of the Vortex Shedding in the Cylinder Wake, Phys. Rev. Lett. **113**, 084501 (2014).
[28] J. M. Cimbala, H. M. Nagib, and A. Roshko, Large structure in the far wakes of two-dimensional bluff bodies, J. Fluid Mech. **190**, 265 (1988).
[29] W. M. Trott, D. J. Rader, J. N. Castañeda, J. R. Torczynski, and M. A. Gallis, Experimental measurements of thermal accommodation coefficients for microscale gas-phase heat transfer, in *Proceedings of the 39th AIAA Thermophysics Conference* (AIAA, Reston, VA, 2007), Paper No. AIAA-2007-4039.
[30] W. M. Trott, D. J. Rader, J. N. Castañeda, J. R. Torczynski, and M. A. Gallis, Measurement of gas-surface accommodation, AIP Conf. Proc. **1084**, 621 (2008).